

On Purely Data-Driven Massive MIMO Detectors

Hao Ye, *Member, IEEE* and Le Liang, *Member, IEEE*

Abstract—To enhance the performance of massive multi-input multi-output (MIMO) detection using deep learning, prior research primarily adopts a model-driven methodology, integrating deep neural networks (DNNs) with traditional iterative detectors. Despite these efforts, achieving a purely data-driven detector has remained elusive, primarily due to the inherent complexities arising from the problem’s high dimensionality. This paper introduces ChannelNet, a simple yet effective purely data-driven massive MIMO detector. ChannelNet embeds the channel matrix into the network as linear layers rather than viewing it as input, enabling scalability to massive MIMO scenarios. ChannelNet is computationally efficient and has a computational complexity of $\mathcal{O}(N_t N_r)$, where N_t and N_r represent the numbers of transmit and receive antennas, respectively. Despite the low computation complexity, ChannelNet demonstrates robust empirical performance, matching or surpassing state-of-the-art detectors in various scenarios. In addition, theoretical insights establish ChannelNet as a universal approximator in probability for any continuous permutation-equivariant functions. ChannelNet demonstrates that designing deep learning based massive MIMO detectors can be purely data-driven and free from the constraints posed by the conventional iterative frameworks as well as the channel and noise distribution models.

I. INTRODUCTION

Massive multi-input multi-output (MIMO) leverages a large number of antennas to improve data rates, coverage, and overall network performance. It plays a pivotal role in enhancing spectral efficiency, making it a cornerstone of 5G and future wireless networks [1], [2]. Nevertheless, handling the increased complexity introduced by massive MIMO, especially in the signal processing pipeline, remains a crucial challenge to fully realize its performance potential. For massive MIMO signal detection, the combination of high-order modulation schemes with a large number of transmit and receive antennas makes exact maximum likelihood (ML) MIMO detection an intractable problem. Given N_t transmit antennas and a modulation of M symbols, the exact estimator has an exponential decoding complexity $\mathcal{O}(M^{N_t})$. Consequently, crafting an efficient and low-complexity symbol detector for massive MIMO represents a critical challenge, which is the central focus of this paper.

There has been extensive research focused on designing efficient massive MIMO detectors [2], [3], [4]. While simple linear detectors, including zero-forcing (ZF) and minimum mean-squared error (MMSE), have low complexity and perform well in smaller systems, they exhibit poor performance compared to ML detectors in larger systems and with higher

order of modulation. In addition to linear detectors, iterative detectors aim to approximate the ML performance with moderate complexity. Approximate message passing (AMP) is asymptotically optimal for large MIMO systems with independent and identically distributed (i.i.d.) Gaussian channels but degrades significantly under realistic ill-conditioned channels. Orthogonal AMP (OAMP) relaxes the i.i.d. Gaussian assumption, but it involves larger computations due to the need for inverse matrix calculations in each iteration [5].

Recently, several learning-based massive MIMO detection schemes, such as OAMPNet [6] and MMNet [7], [8], have emerged by unfolding iterative detectors [9]. These approaches introduce a few amount of trainable parameters into the iterative detectors, which are optimized via minimizing an objective function over datasets. As they need to build on top of existing detection algorithms, these methods are often named as model-driven approaches. While these model-driven methods showcase improvements over their corresponding iterative detectors, their performance is significantly influenced by the original iterative techniques. Other model-driven detectors, employing iterative sampling [10], projection descent [11], and inference frameworks [12], have also been proposed. However, these models tend to be computationally intensive and rely on assumptions about channels and noise, potentially impacting their effectiveness in real-world channel conditions.

In order to fully leverage the power of deep learning, a purely data-driven learning based detector is desired, which is not constrained by the existing iterative detector architectures or assumptions on the channel and noise distribution. However, addressing this challenge is complicated by the high-dimensional nature of the channel matrix \mathbf{H} . While naively training deep neural networks (DNNs) using the channel matrix \mathbf{H} and received signals \mathbf{y} as input to predict transmitted signals \mathbf{x} may work for small-scale MIMO and low modulation schemes (e.g., 4×4 MIMO with quadrature phase shift keying (QPSK) modulation [13]), it fails to scale effectively to massive MIMO scenarios with higher-order modulations.

Therefore, a fundamental yet open challenge in massive MIMO detection is

How to design purely data-driven massive MIMO detectors?

In this paper, we attempt to answer this question and present ChannelNet, a purely data-driven massive MIMO detector. In contrast to model-driven detectors, ChannelNet’s architecture is exclusively crafted from readily available DNN components. It iteratively updates and exchanges features for transmit and receive antennas. In each iteration, the features for each antenna undergo identical and independent updates using a multi-layer perceptron (MLP) model. For feature exchange, we embed the channel matrix \mathbf{H} into the network as linear layers, facilitating exchange between transmit and receive antenna

H. Ye is with the Department of Electrical and Computer Engineering, University of California, Santa Cruz, CA, USA. (e-mail: yehao@ucsc.edu)

L. Liang is with the National Mobile Communications Research Laboratory, Southeast University, Nanjing 210096, and also with the Purple Mountain Laboratories, Nanjing 211111, China (e-mail: lliang@seu.edu.cn).

features.

ChannelNet has demonstrated effectiveness in both theoretical and empirical evaluations. Theoretically, we analyze its expressive power based on MLP models. ChannelNet is proven to be a universal approximator in probability for any continuous permutation-equivariant algorithms in the massive MIMO detection problem, including the ML detection algorithm. This ensures that, with sufficient model size and training data, ChannelNet has the capability to learn and fit any detection algorithms arbitrarily well. In our experimental evaluations, we compare ChannelNet with state-of-the-art detectors across various configurations in terms of antenna numbers, modulation orders, and channel distributions. ChannelNet consistently outperforms or matches these state-of-the-art detectors in all tested scenarios.

In addition to demonstrating superior performance, ChannelNet stands out with several notable advantages when compared to existing approaches:

- **Computational Efficiency:** ChannelNet excels in computational efficiency with a complexity of $\mathcal{O}(N_t N_r)$, where N_t and N_r denote the number of transmit and receive antennas, respectively.
- **No Requirement for Noise Power Input:** In contrast to most existing detectors that necessitate knowledge of the noise power, ChannelNet operates independently of noise power requirements. This characteristic simplifies implementation and alleviates the need for explicit noise power estimation.
- **Robustness:** ChannelNet demonstrates enhanced robustness compared to the model-driven approaches when applied in new environments. Unlike model-driven approaches that rely on maintaining accurate models, ChannelNet's data-driven nature allows it to adapt to novel environment and perform effectively in scenarios where conventional models may struggle to generalize.

In summary, our contributions can be outlined as follows:

- We demonstrate the feasibility of an efficient purely data-driven massive MIMO detector. By leveraging off-the-shelf neural networks, our detector is trained without reliance on conventional iterative frameworks or assumptions about channel and noise distributions.
- We establish the theoretical foundation for ChannelNet as a universal approximator in probability for continuous permutation-equivariant functions, showcasing its versatility and power.
- Through extensive experiments, we empirically validate the effectiveness of ChannelNet across diverse configurations, encompassing varying antenna numbers, modulation orders, and channel distributions.

The rest of this paper is organized as follows. In Section II, we provide preliminaries, including problem formulation and existing detection algorithms. In Section III, we present the proposed data-driven massive MIMO detector, ChannelNet. The analysis of the expressive power of ChannelNet is provided in Section IV. We validate our results with numerical experiments in Section V and we conclude this paper with Section VI.

II. PRELIMINARIES

A. Notation

We use lowercase symbols for scalars, bold lowercase symbols for column vectors and bold uppercase symbols to denote matrices. \mathbf{x}_i represents the i -th element of the vector \mathbf{x} . \mathbf{H}_{ij} denotes the i, j -th element of the matrix \mathbf{H} . \mathbf{H}_i and $\mathbf{H}_{:j}$ refer to the i -th row and j -th column of the matrix \mathbf{H} , respectively. Unless mentioned otherwise, the superscript t on functions, vectors, and matrices denotes the iteration step. I_n stands for identity matrix of size n .

B. Massive MIMO Detection Problem

Consider an uplink scenario in which a massive MIMO base station with N_r antennas serves N_t single-antenna users, where $N_t \leq N_r$. We assume a frequency-flat channel, and the channel coefficients between the N_t transmit antennas and the N_r receive antennas are represented by the matrix $\tilde{\mathbf{H}} \in \mathbb{C}^{N_r \times N_t}$, where $\tilde{\mathbf{H}}_{ij}$ denotes the channel from the j th transmit antenna to the i th receive antenna. The N_t users transmit their symbols individually, forming a symbol vector $\tilde{\mathbf{x}} \in \mathbb{C}^{N_t}$, with each symbol belonging to a constellation $\tilde{\mathcal{X}}$. In this paper, we primarily focus on square quadrature amplitude modulations (QAMs) and symbols are normalized to attain unit average power. It is assumed that the constellation is the same for all transmitters and each symbol has the same probability of being chosen by the users. The received vector $\tilde{\mathbf{y}} \in \mathbb{C}^{N_r}$ results from the symbols transmitted through the channel $\tilde{\mathbf{H}}$ and is affected by additive noise $\tilde{\mathbf{n}}$. This relationship is expressed as:

$$\tilde{\mathbf{y}} = \tilde{\mathbf{H}}\tilde{\mathbf{x}} + \tilde{\mathbf{n}}. \quad (1)$$

Throughout this study, we adopt an equivalent real-valued representation achieved by separately considering the real $\Re(\cdot)$ and imaginary $\Im(\cdot)$ parts. Let $\mathbf{x} = [\Re(\tilde{\mathbf{x}})^T, \Im(\tilde{\mathbf{x}})^T]^T \in \mathbb{R}^K$, $\mathbf{y} = [\Re(\tilde{\mathbf{y}})^T, \Im(\tilde{\mathbf{y}})^T]^T \in \mathbb{R}^N$, $\mathbf{n} = [\Re(\tilde{\mathbf{n}})^T, \Im(\tilde{\mathbf{n}})^T]^T \in \mathbb{R}^N$, and

$$\mathbf{H} = \begin{bmatrix} \Re(\tilde{\mathbf{H}}) & -\Im(\tilde{\mathbf{H}}) \\ \Im(\tilde{\mathbf{H}}) & \Re(\tilde{\mathbf{H}}) \end{bmatrix} \in \mathbb{R}^{N \times K}, \quad (2)$$

where $K = 2N_t$ and $N = 2N_r$. This allows us to express the system in the equivalent real-valued form as follows:

$$\mathbf{y} = \mathbf{H}\mathbf{x} + \mathbf{n}. \quad (3)$$

Massive MIMO detectors aim to determine the transmitted vector \mathbf{x} in real-value representation constellation \mathcal{X}^K based on the received vector \mathbf{y} and the channel matrix \mathbf{H} , which is typically assumed to be known at the receiver but not at the transmitter. Formally, the massive MIMO detection problem involves solving the combinatorial optimization problem:

$$\underset{\mathbf{x} \in \mathcal{X}^K}{\operatorname{argmin}} \|\mathbf{y} - \mathbf{H}\mathbf{x}\|^2, \quad (4)$$

which is NP-hard due to the finite constellation constraint. The ML detector serves as an optimal algorithm for solving the MIMO detection problem, employing an exhaustive search that assesses all possible signals in the constellation. However, the complexity of ML is exponential in the number of transmitted data streams, rendering it impractical for massive MIMO scenarios.

C. Linear MIMO Detectors

Linear detectors, such as ZF and MMSE detectors, are characterized by their lower computational complexity. However, their performance is not on par with the optimal ML detector. These linear detectors operate by multiplying the received signal vector \mathbf{y} with an equalization matrix \mathbf{A}^T . Subsequently, the output undergoes quantization through a slicer denoted as $\mathcal{S}(\cdot)$, which quantizes each entry to the nearest neighbor in the constellation. The overall operation of linear detectors can be expressed as $\hat{\mathbf{x}} = \mathcal{S}(\mathbf{A}^T \mathbf{y})$.

ZF Detector: The ZF detector operates by inverting the channel matrix \mathbf{H} to eliminate its impact. The equalization matrix of the ZF detector is the pseudo-inverse of the channel matrix, which is given by

$$\mathbf{A}_{\text{ZF}} = (\mathbf{H}^T \mathbf{H})^{-1} \mathbf{H}^T. \quad (5)$$

Linear MMSE Detector: The linear MMSE detector accounts for the influence of noise in its operation by incorporating additional information about the noise power. The equalization matrix for the MMSE detector is defined as

$$\mathbf{A}_{\text{MMSE}} = (\mathbf{H}^T \mathbf{H} + \sigma^2 \mathbf{I}_K)^{-1} \mathbf{H}^T, \quad (6)$$

where σ is the noise power. This approach effectively mitigates the noise enhancement problem inherent in the ZF detector, allowing the MMSE detector to achieve improved performance, especially in scenarios with significant noise power.

D. Iterative MIMO Detectors

Iterative MIMO detectors aim to approximate the ML solution with iterations. Many iterative detectors fall in the general framework with the following two steps in each iteration.

$$\mathbf{u}^t = \mathbf{x}^t + \mathbf{A}^t (\mathbf{y} - \mathbf{H} \mathbf{x}^t) + \mathbf{b}^t, \quad (7)$$

$$\mathbf{x}^{t+1} = \eta^t(\mathbf{u}^t, \sigma_0). \quad (8)$$

The first step involves a linear transformation, resulting in an intermediate signal \mathbf{u}^t in a continuous domain. The second step employs a non-linear denoiser $\eta^t(\cdot)$ to process the intermediate signal, yielding the estimation \mathbf{x}^{t+1} for the next iteration. The goal is to improve the estimation \mathbf{x}^t gradually through iterations.

Approximate message passing (AMP): AMP is an iterative detection algorithm designed to be asymptotically optimal in large MIMO systems with i.i.d. Gaussian channels [14]. It leverages approximate inference in a graphical model representation of the MIMO system. AMP can be seen as a specific case within the iterative framework, using $\mathbf{A}^t = \mathbf{H}^T$ as the linear operator and \mathbf{b}^t as the Onsager term. While AMP excels with i.i.d. Gaussian channels and its lower complexity, its performance deteriorates for other channel matrices, particularly those that are ill-conditioned or spatially correlated.

Orthogonal AMP (OAMP): OAMP was introduced to relax the constraints on channel matrices posed by AMP [5]. Specifically designed for unitary-invariant matrices [15], OAMP extends its applicability to a broader range of scenarios beyond the limitations of AMP. OAMP can also be considered as a specific case within the iterative framework. It does not

include \mathbf{b}^t but \mathbf{A}^t is much more complicated, which involves computing a matrix pseudo inverse at each iteration.

Semidefinite Relaxation (SDR): SDR offers a computationally efficient approximation for the ML detector by proposing a convex relaxation of the ML problem [16]. As the ML detector involves non-convex optimization with high complexity, SDR provides a convex (semidefinite) program approximation that can be solved in polynomial time.

Sphere Decoder: The sphere decoder (SD) is an efficient search algorithm that prunes the search space based on a defined radius [17]. However, even with the use of SD, the expected computational complexity remains exponential and impractical for many applications.

E. Model-Driven Learning-Based Detectors

Most existing learning-based massive MIMO detectors can be categorized as model-driven, wherein domain knowledge is integrated into the architecture to facilitate the training of neural networks. However, this approach can render the model less flexible and susceptible to biases inherited from its parent algorithm.

DetNet: DetNet is a model-driven detector by applying iterative projected gradient descent [11]. DetNet matches the performance of SDR on i.i.d. Gaussian channels with low-order modulation schemes, but it degrades for correlated channels and higher order modulations.

OAMPNet: OAMPNet is a model-driven detector based on the OAMP algorithm [6]. It incorporates two learnable parameters, *i.e.*, γ_t and v_t , per iteration of the OAMP algorithm. As OAMPNet is based on the OAMP algorithm, it also makes the strong assumption that the channel matrices are unitary-invariant. Similar to OAMP, OAMPNet also requires computing a matrix pseudo inverse at each iteration, resulting in complexity higher than its alternatives such as AMP.

MMNet: MMNet [7] is another model-driven detector based on the iterative soft-thresholding algorithm [18]. MMNet follows the iteration framework (7) by replacing \mathbf{A}^t with a matrix of learning parameters, setting $\mathbf{b}^t = 0$, and adding a vector of learning parameters to the noise estimation in the denoiser. Although its performance is comparable to the ML for Rayleigh fading channels, MMNet requires online training for each channel realization in the case of correlated channels. Consequently, its applicability is limited for real-time applications.

RE-MIMO: RE-MIMO [12] is a detector following the Recurrence Inference Machine framework [19] that achieves state-of-the-art performance for correlated channel models. It is an iterative detector with two steps. Each iteration is composed by an encoder step, parameterized by a transformer, and a predictor module, which plays the role of the denoiser. In addition to its good performance, the detector can handle a varying number of transmitters using the same trained model.

III. METHOD

A. ChannelNet Detector Architecture

The ChannelNet architecture, depicted in Fig. 1 (a), operates through iterative updates and exchanges of transmit and receive antenna features, denoted as $\mathbf{F}_{tx} = [\mathbf{f}_1^{tx}, \dots, \mathbf{f}_i^{tx} \dots \mathbf{f}_K^{tx}] \in$

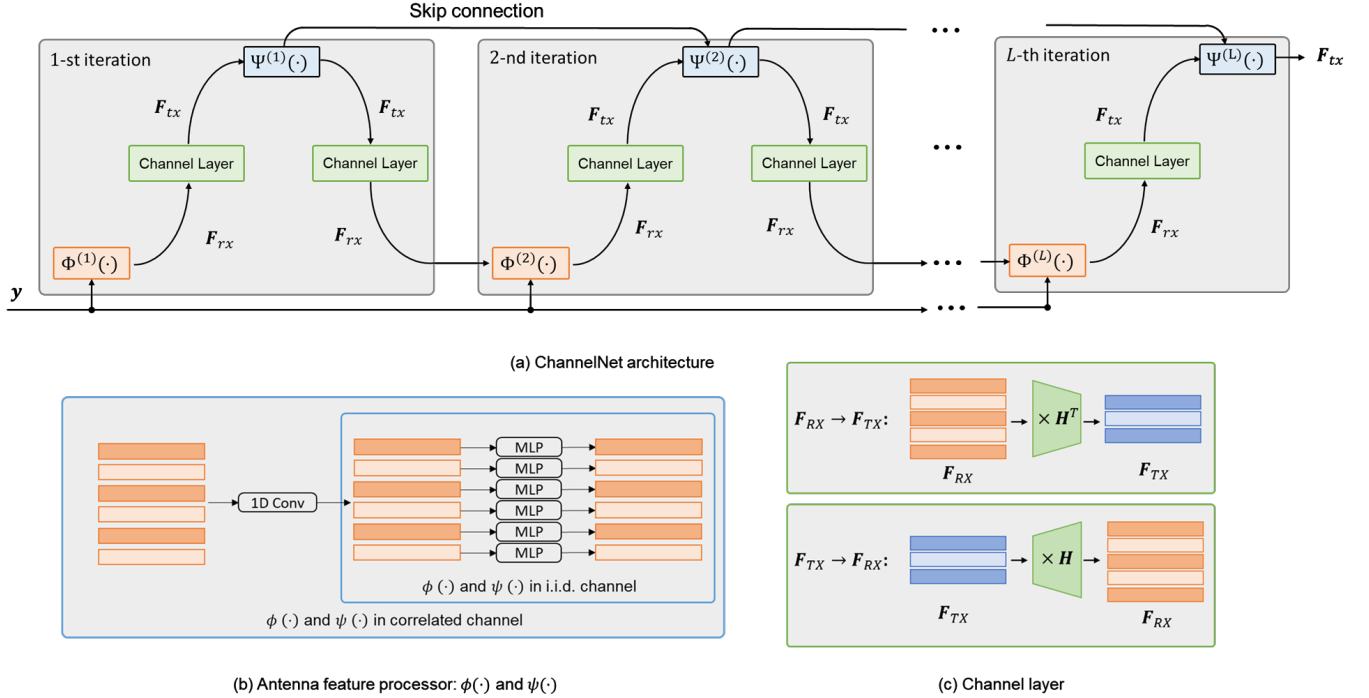


Fig. 1: Proposed architecture: (a) The general iterative framework. (b) The architecture of the antenna feature processor. (c) The channel layer architecture.

$\mathbb{R}^{K \times d}$ and $\mathbf{F}_{rx} = [\mathbf{f}_1^{rx}, \dots, \mathbf{f}_j^{rx}, \dots, \mathbf{f}_N^{rx}] \in \mathbb{R}^{N \times d}$, where $\mathbf{f}_i^{tx}, \mathbf{f}_j^{rx} \in \mathbb{R}^d$ represent feature vectors for the i -th transmit and the j -th receive antenna, respectively. ChannelNet comprises two main components: the antenna feature processor and the channel layer. The transmit antenna feature, \mathbf{F}_{tx} , undergoes updates with the transmit antenna processor $\Psi(\cdot)$, while the receive antenna feature, \mathbf{F}_{rx} , is updated with the receive antenna processor $\Phi(\cdot)$. The channel layer facilitates transformations between transmit and receive antenna features.

In each iteration, the receive antenna feature, \mathbf{F}_{rx} , is first updated with $\Phi(\cdot)$ and then processed through the channel layer to obtain the transmit antenna features. Similarly, the transmit antenna feature, \mathbf{F}_{tx} , is updated with $\Psi(\cdot)$ and then processed through the channel layer, resulting in receive antenna feature, \mathbf{F}_{rx} , for the subsequent iteration. The first iteration uses the receiver data \mathbf{y} as \mathbf{F}_{rx} , and the final iteration concludes with the updated \mathbf{F}_{tx} as the output.

Antenna Feature Processor: The antenna feature processors, $\Phi(\cdot)$ and $\Psi(\cdot)$, play a critical role in ChannelNet, facilitating the transformation of transmit and receive antenna feature in each iteration. As illustrated in Fig. 1 (b), we use different architectures for i.i.d. channels and correlated channels. For i.i.d. channels, the channel distribution is independent of the representation order of the antennas. To ensure the permutation-equivariance of the antenna ordering, local function paradigm [20], [21] is utilized, where the antenna feature vectors are processed identically and individually for each antenna. In specific, each transmit (receive) antenna feature vector is updated with an MLP network, which is shared across the all transmit (receive) antennas. Therefore, for the t -th iteration, two MLP networks need to be learned,

denoted by $\phi^{(t)}(\cdot)$ and $\psi^{(t)}(\cdot)$, and the updating formulation of $\Phi^{(t)}(\cdot)$ and $\Psi^{(t)}(\cdot)$ can be represented as

$$\Phi^{(t)}(\mathbf{F}_{rx}) = [\phi^{(t)}(\mathbf{f}_1^{rx}), \dots, \phi^{(t)}(\mathbf{f}_N^{rx})], \quad (9)$$

$$\Psi^{(t)}(\mathbf{F}_{tx}) = [\psi^{(t)}(\mathbf{f}_1^{tx}), \dots, \psi^{(t)}(\mathbf{f}_K^{tx})]. \quad (10)$$

In the case of correlated channels, the channel distribution is not entirely independent of the representation order of the antennas due to correlations between adjacent antennas. To account for this, additional convolutional layers operating along the antennas are included in the antenna feature processors, as depicted in Fig. 1 (b). This enables the consideration of features from adjacent antennas during the transformation process.

In subsequent discussions, the architectures of ChannelNet for i.i.d. channels and correlated channels are referred to as ChannelNet-MLP and ChannelNet-Conv, respectively.

Channel Layer: The exchange between the transmit and receive antenna features is facilitated through the channel layers. As illustrated in Fig. 1 (c), the channel layer leverages the linear nature of the massive MIMO system, employing linear transformations between the transmit and receive antenna features.

In the transformation from transmit to receive antenna feature, the channel matrix \mathbf{H} is used as the linear transformation coefficients, *i.e.*, $\mathbf{F}_{rx} = \mathbf{H}\mathbf{F}_{tx}$. Conversely, the transpose of \mathbf{H} is utilized as the coefficients for transforming features from receive to transmit antenna feature, *i.e.*, $\mathbf{F}_{tx} = \mathbf{H}^T\mathbf{F}_{rx}$. In this way, the channel matrix \mathbf{H} is embedded as linear layers into the network, eliminating the need for \mathbf{H} as an explicit input. This design effectively addresses the high-dimensionality challenge encountered in previous data-driven MIMO detectors, enabling

ChannelNet to operate efficiently in massive MIMO and high-order modulation scenarios.

Algorithm 1 ChannelNet Detector

```

1: procedure CHANNELNET( $\mathbf{H}, \mathbf{y}$ )
2:    $\mathbf{F}_{rx} \leftarrow \mathbf{y}$ 
3:   for  $t = 1$  to  $L$  do
4:      $\mathbf{F}_{rx} \leftarrow \Phi^{(t)}(\mathbf{F}_{rx})$   $\triangleright$  Receive Feature Processor
5:      $\mathbf{F}_{tx} \leftarrow \mathbf{H}^T \mathbf{F}_{rx}$   $\triangleright$  Channel Layer
6:     if  $l > 1$  then
7:        $\mathbf{F}_{tx} = \mathbf{F}_{tx} + \mathbf{F}_{tx}^{old}$   $\triangleright$  Skip Connection
8:        $\mathbf{F}_{tx}^{old} \leftarrow \mathbf{F}_{tx}$ 
9:        $\mathbf{F}_{tx} \leftarrow \Psi^{(t)}(\mathbf{F}_{tx})$   $\triangleright$  Transmit Feature Processor
10:       $\mathbf{F}_{rx} \leftarrow \mathbf{H} \mathbf{F}_{tx}$   $\triangleright$  Channel Layer
11:       $\mathbf{F}_{rx} \leftarrow \mathbf{F}_{rx} - \mathbf{y} \mathbf{1}_d^T$   $\triangleright$  Subtract  $\mathbf{y}$ 
12:   return  $\mathbf{F}_{tx}$ 

```

Implement Details: There are two detailed designs that are beneficial for the experimental performance of ChannelNet.

- **Skip Connection:** Integrating skip connections is a well-established technique to improve gradient flow, thereby facilitating the training of deep networks by mitigating issues such as vanishing or exploding gradients [22]. As depicted in Fig. 1 (a), skip connections are integrated into the transmit antenna feature processor. Specifically, the input to the transmit antenna feature processor in the t -th iteration is added as input to the transmit antenna feature processor in the $t + 1$ -th iteration.
- **Subtraction of \mathbf{y} :** The received signal \mathbf{y} is beneficial for the updating of the receive antenna features. In addition to using \mathbf{y} as the initial receiver features, \mathbf{y} is also utilized in subsequent iterations for feature transformation. An effective design we have identified is to directly subtract \mathbf{y} from the receive antenna feature \mathbf{F}_{rx} at each feature dimension. Consequently, instead of using \mathbf{F}_{rx} as the input to the receive feature processor, we actually use $\mathbf{F}_{rx} - \mathbf{y} \mathbf{1}_d^T$ as the input, where $\mathbf{1}_d^T$ denotes an all-one vector of size d .

The complete algorithm of ChannelNet is outlined in Algorithm 1.

Training Process: The training process for ChannelNet involves the optimization of a loss function over a training dataset comprising triples of transmit symbols \mathbf{x} , channel matrices \mathbf{H} , and received data \mathbf{y} . Formulated as an M -class classification task, where M denotes the modulation order, the chosen loss function is the cross-entropy loss:

$$L = \sum_{i=1}^K \sum_{j=1}^M p_{i,j} \log(\hat{p}_{i,j}), \quad (11)$$

where $\hat{p}_{i,j}$ represents the predicted probability generated by ChannelNet for the i -th antenna using the j -th symbol in the constellation and the $p_{i,j}$ denotes the groundtruth constructed from the transmit symbols \mathbf{x} .

Computational Complexity: The computation complexity for ChannelNet is $\mathcal{O}(N_r N_t)$. Specifically, the complexity for the MLP model is $\mathcal{O}(d^2)$, where d is the antenna feature

TABLE I: Computational Complexity

Detector	Computation Complexity
AMP	$\mathcal{O}(N_t N_r)$
MMSE	$\mathcal{O}(N_t^3 + N_t^2 N_r)$
OAMPNet	$\mathcal{O}(N_t^3 + N_r^3 + N_t^2 N_r + N_r^2 N_t)$
RE-MIMO	$\mathcal{O}(N_t^2 N_r + N_r^2 N_t)$
ChannelNet	$\mathcal{O}(N_t N_r)$

dimension. As a result, the complexities for the the transmit and receive antenna processors are $\mathcal{O}(d^2 N_r)$ and $\mathcal{O}(d^2 N_t)$, respectively. When additional convolutional layers are used, the computation complexity for the convolution layers is $\mathcal{O}(k d^2 N_t) + \mathcal{O}(k d^2 N_r)$, where k denotes the kernel size. The computation complexity for the channel layer involves two matrix multiplications, resulting in $\mathcal{O}(d N_t N_r)$. Therefore, the overall computation complexity per iteration is $\mathcal{O}(d^2 N_r) + \mathcal{O}(d^2 N_t) + \mathcal{O}(d N_r N_t)$, which grows linearly with the product of N_r and N_t .

For a comprehensive understanding, we provide a comparison of the computational complexities of existing approaches in Table I. From the table, AMP shares the same complexity order as ChannelNet, both at $\mathcal{O}(N_t N_r)$, primarily due to channel matrix and residual vector multiplication. In contrast, the MMSE scheme exhibits higher complexities at $\mathcal{O}(N_t^3 + N_t^2 N_r)$ due to the need for matrix pseudo inversion. Similarly, OAMPNet, requiring matrix pseudo inversion at each iteration, has a complexity of $\mathcal{O}(N_t^3 + N_r^3 + N_t^2 N_r + N_r^2 N_t)$. RE-MIMO requires $\mathcal{O}(N_t^2 N_r + N_r^2 N_t)$ per iteration. Beyond the $\mathcal{O}(\cdot)$ analysis, Section V delves into a comparison of the number of multiplication operations required per signal detection.

IV. EXPRESSIVE POWER ANALYSIS

In this section, we analyze the expressive power analysis of ChannelNet-MLP, emphasizing its ability to approximate any continuous permutation-equivariant functions. We begin by introducing the concept of permutation-equivariant functions in the context of massive MIMO detection. Subsequently, we present our main result, demonstrating that ChannelNet is a universal permutation-equivariant approximator in probability.

A. Permutation Equivariant Functions

Group equivariant functions are those in which the input and output maintain a specific relationship with transformations defined over a group. Let X and Y be the input and output vector spaces, respectively, both of which are endowed with a set of transformations $G : G \times X \rightarrow X$ and $G \times Y \rightarrow Y$. A function $f : X \rightarrow Y$ is called equivariant with respect to G if when any transformation is applied to the input, the output also changes via the same transformation or under a certain predictable behavior. Formally, we have the following definition:

Definition 1 (Group Equivariant Function) *Let X and Y be the input and output vector spaces, respectively, both of which are endowed with a set of transformations $G : G \times X \rightarrow X$ and $G \times Y \rightarrow Y$. The function $f : X \rightarrow Y$ is called equivariant with respect to G if*

$$f(\rho_X(g)x) = \rho_Y(g)f(x) \quad \forall g \in G, \quad (12)$$

where ρ_X and ρ_Y are the group representations in the input and output space, respectively. Specifically, f is called invariant if ρ_Y is the identity.

In massive MIMO detection, our focus is on permutation groups associated with transmit and receive antennas. Let \mathcal{S}_N and \mathcal{S}_K denote all permutations for the receive antennas and the transmit antennas, respectively. For any $\sigma_{tx} \in \mathcal{S}_K$, represented by its corresponding permutation matrix \mathbf{P}_{tx} , the permutation of the transmit antennas is expressed as the permutation of the columns of the channel matrix, i.e., $\sigma_{tx}(\mathbf{H}) = \mathbf{H}\mathbf{P}_{tx}$. For any $\sigma_{rx} \in \mathcal{S}_N$, represented by its corresponding permutation matrix \mathbf{P}_{rx} , the permutation of the receive antennas is expressed as the permutation of both the rows of the channel matrix and the received signal, i.e., $\sigma_{rx}(\mathbf{H}, \mathbf{y}) = (\mathbf{P}_{rx}\mathbf{H}, \mathbf{P}_{rx}\mathbf{y})$.

A function is called permutation-equivariant if it remains unchanged with every receive antenna permutation and changes equivariantly with every transmit antenna permutation. The formal definition is provided below.

Definition 2 (Permutation Equivariant Function) A function $f : \mathbb{R}^{N \times K} \times \mathbb{R}^N \rightarrow \mathbb{R}^K$ is said to be permutation equivariant if for every $\sigma_{rx} \in \mathcal{S}_N, \sigma_{tx} \in \mathcal{S}_K$, it satisfies

$$\sigma_{tx}(f(\mathbf{H}, \mathbf{y})) = f((\sigma_{rx}, \sigma_{tx}) * (\mathbf{H}, \mathbf{y})) \quad (13)$$

where $(\sigma_{rx}, \sigma_{tx}) * (\mathbf{H}, \mathbf{y})$ represents the channel matrix and the receive signal after applying permutation $(\sigma_{rx}, \sigma_{tx})$.

Notably, ChannelNet-MLP achieves permutation equivariance due to the independent processing of antenna functions and linear exchange functions. Conversely, ChannelNet-Conv lacks permutation equivariance as the convolution layer depends on the antenna order.

B. Universal Permutation Equivariant Approximator

Universal approximators are mathematical models or systems that have the capacity to closely approximate any given function within a specified class. It is well-known that MLP is an universal approximator for any continuous functions [23], [24]. Building upon MLP, ChannelNet-MLP is clearly not an universal approximator for any continuous functions, as it can only represent permutation-equivariant functions. A natural question to ask is if it can approximate any permutation-equivariant function. Unfortunately, it is not true as demonstrated in the following example:

Counterexample: Consider the following two channel matrices and received signals:

$$\mathbf{H}_1 = \begin{bmatrix} 1, & 0 \\ 0, & 1 \end{bmatrix}, \mathbf{y}_1 = [0, 0]^T,$$

$$\mathbf{H}_2 = \begin{bmatrix} 0.5, & 0.5 \\ 0.5, & 0.5 \end{bmatrix}, \mathbf{y}_2 = [0, 0]^T.$$

If ChannelNet-MLP is applied to both cases, the outputs are identical regardless of the functions used to represent the transmit and receive feature processors. This is due to the received data is same for each antenna and the fact that each row and

column in \mathbf{H}_1 and \mathbf{H}_2 has a summation of 1, making the two cases indistinguishable from the perspective of each antenna. Specifically, in the first iteration, the receive antenna feature vectors are $\mathbf{f}_1^{rx} = \mathbf{f}_2^{rx} = [\phi^{(1)}(0), \phi^{(1)}(0)]$ after the receiver feature update module. Subsequently, the transmit antenna feature vectors after the channel layer are identical to the receive antenna feature vectors, i.e., $\mathbf{f}_1^{tx} = \mathbf{f}_2^{tx} = [\phi^{(1)}(0), \phi^{(1)}(0)]$, due to the summation of every channel column is 1. Using the transmit antenna processor, the features are transformed into $\mathbf{f}_1^{tx} = \mathbf{f}_2^{tx} = [\psi^{(1)} \circ \phi^{(1)}(0), \psi^{(1)} \circ \phi^{(1)}(0)]$ for both cases. The receive antenna features obtained after the channel layer are also $\mathbf{f}_1^{rx} = \mathbf{f}_2^{rx} = [\psi^{(1)} \circ \phi^{(1)}(0), \psi^{(1)} \circ \phi^{(1)}(0)]$, due to the summation of every channel row is 1. Subsequent iterations follow the same pattern, and neither the antenna feature processors nor the channel layers can distinguish between these two scenarios. In essence, ChannelNet-MLP cannot differentiate these cases, making it unable to approximate a permutation-equivariant detector that produces distinct outputs for them.

However, it is important to note that such scenarios are rare in real-world communication systems and can be considered negligible. The primary reason ChannelNet cannot differentiate between the two cases in the aforementioned example is because both the received data and the sum of channel gains being identical. In practical communication systems, channel gains and received data are derived from continuous distributions and therefore identical received data or symmetric channel gain cases have probability of 0. In the subsequent theorem, we establish that for any continuous distribution of channel matrices and received data, ChannelNet can approximate any permutation-equivariant detector with probability 1.

Theorem 1 Let X be a compact set in $\mathbb{R}^{N \times (K+1)}$, and P be a Borel probability measure over X . Consider any continuous permutation-equivariant function g . For any given $\epsilon > 0$ and $0 < \delta < 1$, there exists a function f represented by ChannelNet-MLP, such that

$$P(\|g(\mathbf{H}, \mathbf{y}) - f(\mathbf{H}, \mathbf{y})\| < \epsilon) > 1 - \delta, (\mathbf{H}, \mathbf{y}) \in X. \quad (14)$$

All proofs are deferred to the Appendix.

This theorem highlights the richness of the function space represented by ChannelNet-MLP, making it capable of distinguishing any continuous permutation-equivariant functions. In the context of the MIMO detection problem, ML detection serves as the upper bound. Despite ML detection not being a continuous function due to its discrete output, the following corollary demonstrates that ChannelNet-MLP can approximate the ML detector arbitrarily well.

Corollary 1 Let X be a compact set in $\mathbb{R}^{N \times (K+1)}$, and P be a Borel probability measure over X . For any given $\epsilon > 0$ and $0 < \delta < 1$, there exists a function $f : X \rightarrow \mathbb{R}^K$ represented by ChannelNet-MLP, such that

$$P(\|f_{ML}(\mathbf{H}, \mathbf{y}) - f(\mathbf{H}, \mathbf{y})\| < \epsilon) > 1 - \delta, (\mathbf{H}, \mathbf{y}) \in X, \quad (15)$$

where f_{ML} denotes the ML detector.

V. EXPERIMENTS

In this section, we present numerical results to evaluate and compare the performance of ChannelNet with other state-of-the-art MIMO detection schemes. We use the symbol error rate (SER) as the performance evaluation metric in our experiments. We evaluate the SER under various conditions, including modulation order, channel distributions, and noise distributions. Below we discuss the implementation details of the detection schemes used in our experiments.

- **MMSE:** Classical linear receiver that inverts the signal by applying the channel-noise regularized pseudoinverse of the channel matrix and rounds the output to the closest point on the constellation.
- **AMP:** AMP algorithm with 50 iterations since the performance does not improve with more iterations[7].
- **V-BLAST:** Multi-stage successive interference cancellation BLAST algorithm with ZF detector.
- **ML:** The optimal detector, implemented using Gurobi [25] optimization package.
- **DetNet:** Learning based detector with $3N_t$ layers as introduced in [11].
- **OAMPNet:** OAMPNet unrolls OAMP iterations with 10 layers and 2 learnable parameters per layer [6].
- **Re-MIMO:** A model-driven detector based on an encoder-predictor architecture [12]. Encoder parameterized by a transformer, predictor with an MLP.
- **ChannelNet-MLP:** ChannelNet-MLP with 20 iterations is used. The feature dimension $d = 10$ is used. The MLP networks for the antenna feature processors contain 2 linear layers, where the number of neurons in each layer is also 10. The network is trained with 600 epochs, and epoch contains 2×10^6 samples of $(\mathbf{x}, \mathbf{H}, \mathbf{y})$. We use batch size 64 and Adam optimizer [26] with momentum 0.9. The initial learning rate is 10^{-3} , which is decreased by factor 0.1 every 200 epochs.
- **ChannelNet-Conv:** The MLP network architecture remains the same with ChannelNet-MLP, with 2 convolutional layer added to each antenna feature processor. In each convolutional layer, kernel size of 3 is used and the number of filters is 10.

For all the experiments in the following subsections, we consider two different modulation schemes, *i.e.*, 16-QAM and 64-QAM. Two antenna setting are considered, *i.e.*, $(N_r, N_t) = (64, 32)$ and $(N_r, N_t) = (128, 64)$. Two types of channel are used for evaluation, *i.e.*, Rayleigh fading channel and the correlated channels. The channel noise follows i.i.d. zero-mean Gaussian distribution if not specifically stated and the noise power is determined by the SNR as per the formula

$$\text{SNR} = \frac{\mathbb{E}[\|\mathbf{H}\mathbf{x}\|_2^2]}{\mathbb{E}[\|\mathbf{n}\|_2^2]}. \quad (16)$$

Notably, ChannelNet does not require explicit noise input, in contrast to the baselines, which require noise power inputs—except for ML.

A. Rayleigh Fading Channel

In this subsection, we consider a Rayleigh Fading Channel where each element \mathbf{H} follows a zero-mean circularly-

symmetric Gaussian distribution with variance $1/N_r$, *i.e.*, $\mathbf{H}_{ij} \sim \mathcal{CN}(0, 1/N_r)$.

Fig. 2 presents a comprehensive comparison of the SER for ChannelNet and other detectors in scenarios involving 16-QAM and 64-QAM modulations with $(N_r, N_t) = (64, 32)$. Remarkably, ChannelNet consistently outperforms or matches existing detectors, and its performance is close to the ML bound, showcasing its efficiency in approximating optimal performance.

Fig. 3 depicts the comparison of the SER with $(N_r, N_t) = (128, 64)$. Re-MIMO and ML performances are excluded due to challenges in scaling these approaches to this specific antenna setting. The observed trends align consistently with the performance observed under the $(N_r, N_t) = (64, 32)$ configuration, once again demonstrating that ChannelNet can either match or surpass existing detectors. This reaffirms the robust performance of ChannelNet across varying antenna configurations. Moreover, the scalability of ChannelNet with the number of antennas underscores the effectiveness of the channel embedding layer, which enables data-driven methods to work effectively in scenarios with a large number of antennas.

B. Correlated channel

In this subsection, we consider correlated MIMO channels using the Kronecker model:

$$\mathbf{H} = \mathbf{R}_R^{1/2} \mathbf{H}_w \mathbf{R}_T^{1/2}, \quad (17)$$

where \mathbf{H}_w is the channel matrix under Rayleigh fading channel, and \mathbf{R}_R and \mathbf{R}_T are the spatial correlation matrix at the receiver and transmitter side, respectively. These matrices are generated according to the exponential correlation model [27]. In this experiment, we fix correlation coefficient ρ at 0.6.

In Fig. 4, we present the SER performance for two antenna configurations: $(N_r, N_t) = (64, 32)$ and $(N_r, N_t) = (128, 64)$. The comparison includes both ChannelNet-MLP and ChannelNet-Conv. ChannelNet demonstrates its efficacy in handling correlated channels. ChannelNet-MLP exhibits comparable performance to OAMPNet. Notably, the addition of a convolutional layer in ChannelNet-Conv results in a significant performance improvement, surpassing all baseline methods by 1-2 dB.

C. Robustness

In this subsection, we address the critical issue of robustness in machine learning approaches, specifically examining how well detectors generalize to test environments differing from their training sets. This analysis provides valuable insights into the robustness of ChannelNet in scenarios beyond its training environment. We conduct evaluations using a Rayleigh fading channel with $(N_r, N_t) = (64, 32)$ and 16-QAM modulation. It is worth noting that ChannelNet exhibits nearly identical performance compared to OAMPNet and Re-MIMO under consistent training and test conditions, as shown in Fig. 2. Therefore, any differences observed in the new environment are attributable to the generalization ability of each detector.

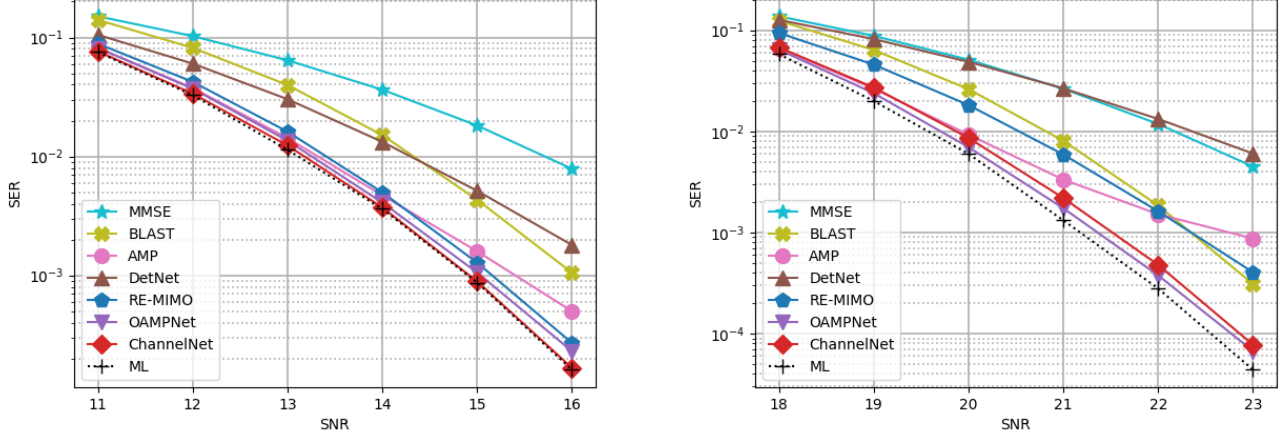


Fig. 2: The SER performance comparison for $(N_r, N_t) = (64, 32)$ with 16-QAM (left) and 64-QAM (right) under Rayleigh Fading Channel.

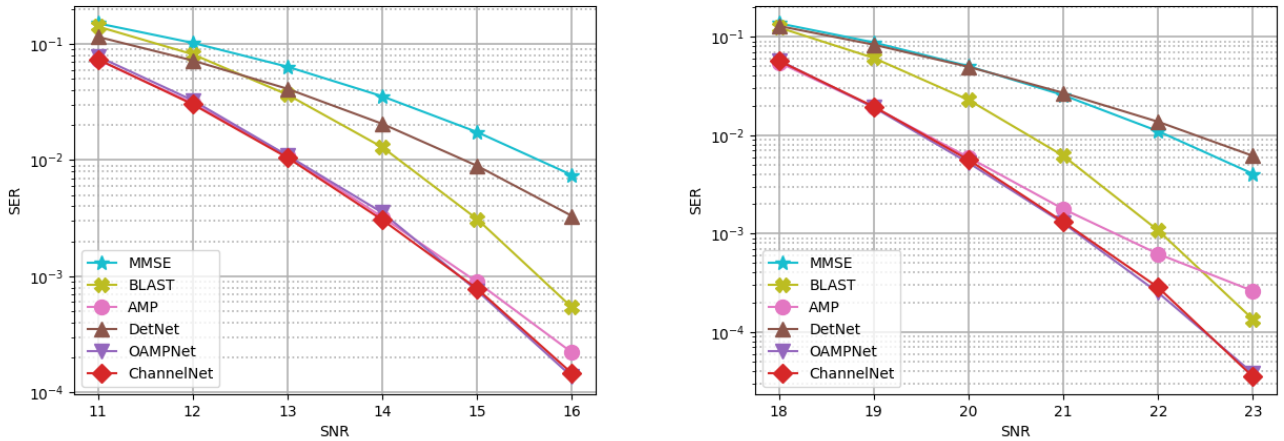


Fig. 3: The SER performance comparison for $(N_r, N_t) = (128, 64)$ with 16-QAM (left) and 64-QAM (right) under Rayleigh Fading Channel.

1) *Channel Estimation Noise*: In many wireless communication systems, obtaining perfect channel state information (CSI) at the receiver is often impractical. In such scenarios, the receiver operates based on a noisy estimate of the true channel, introducing uncertainties during signal demodulation. To emulate this imperfect CSI situation, we model the channel matrix \mathbf{H} with additional AWGN before it reaches the receiver for demodulation. The perturbed channel is expressed as:

$$\hat{\mathbf{H}} = \mathbf{H} + \mathbf{E} \quad (18)$$

where $\hat{\mathbf{H}}$, \mathbf{H} , and \mathbf{E} represent the perturbed channel, the true channel matrix, and the channel estimation error, respectively. Each element of \mathbf{E} is drawn from a zero-mean i.i.d. Gaussian distribution, whose variance is determined by the $\text{SNR}_{\mathbf{H}}$:

$$\text{SNR}_{\mathbf{H}} = \frac{\|\mathbf{H}\|_F^2}{\|\mathbf{E}\|_F^2}, \quad (19)$$

where $\|\cdot\|_F$ denotes the Frobenius norm.

In our experiments, we intentionally introduce channel estimation errors to assess the robustness of detectors. We set the $\text{SNR}_{\mathbf{H}}$ at two levels, namely 15 dB and 20 dB. Fig. 5 (a) illustrates the SER performance of ChannelNet, OAMPNet, and Re-MIMO under these conditions. Notably, ChannelNet demonstrates superior generalization capabilities compared to Re-MIMO and OAMPNet, at both estimation noise levels.

2) *Non-Gaussian Channel Noise*: The Gaussian noise model, while accurate for various scenarios such as thermal noise, falls short in capturing the characteristics of disturbances prevalent in certain communication channels like urban, indoor, and underwater acoustic environments. In these cases, atmospheric and man-made electromagnetic noises introduce non-Gaussian characteristics, often exhibiting impulsive behavior and heavy-tailed probability density functions.

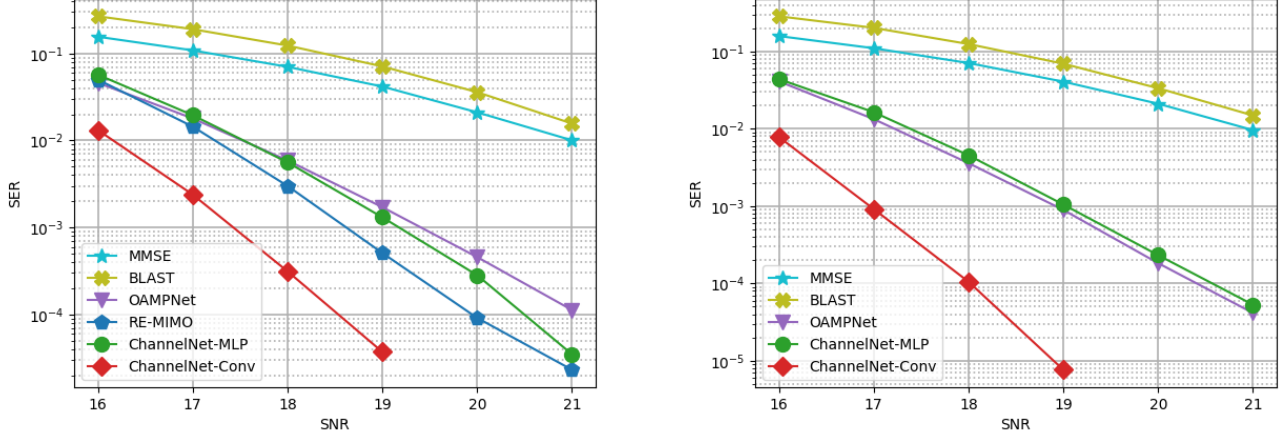


Fig. 4: The SER performance comparison for $(N_r, N_t) = (64, 32)$ (left) and $(N_r, N_t) = (128, 64)$ (right) with 16-QAM correlated Channel.

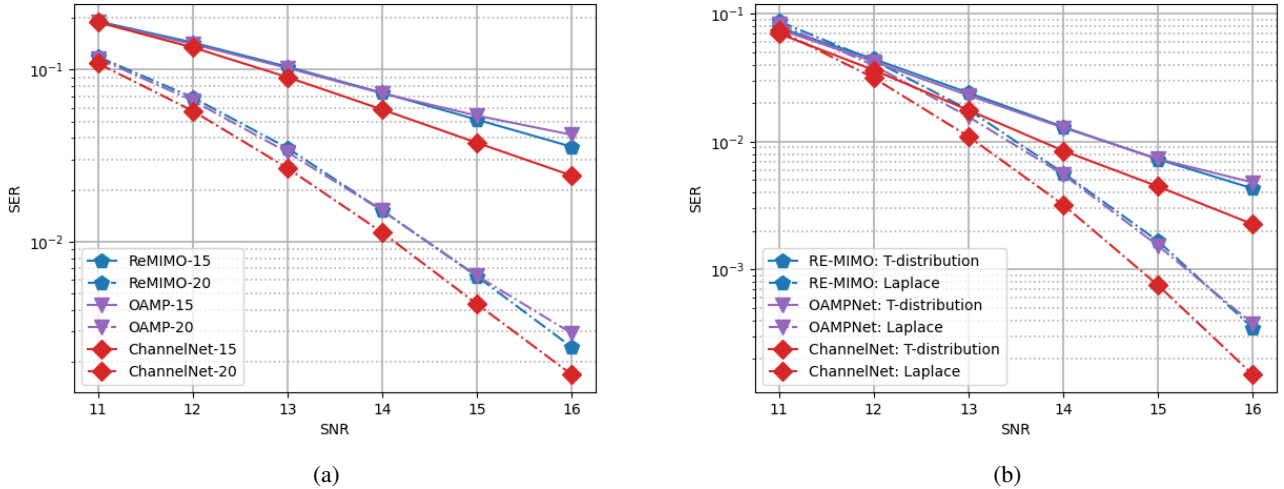


Fig. 5: The SER performance with channel estimation error (left) and non-Gaussian noise (right).

To assess ChannelNet’s robustness to non-Gaussian noise, we specifically consider the t-distribution family characterized with the parameter $\nu = 3$ and the Laplace distribution. Fig. 5 (b) presents the SER performance of ChannelNet, OAMPNet, and Re-MIMO under these conditions. Remarkably, ChannelNet demonstrates superior generalization capabilities compared to Re-MIMO and OAMPNet, showcasing its robustness in the presence of non-Gaussian noise distributions.

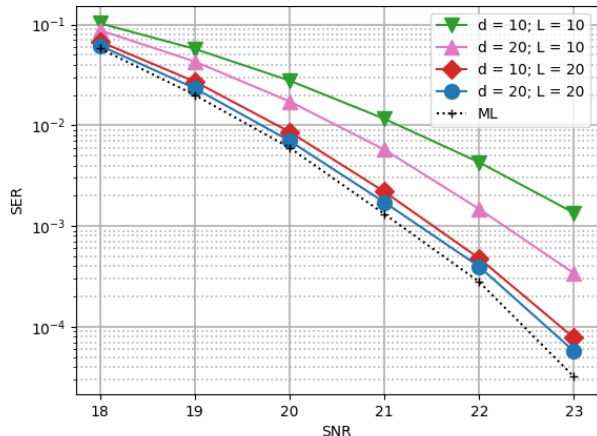
D. Tradeoff between Model Size and Performance

ChannelNet is a purely data-driven method with standard deep learning components, allowing for easy adjustments to the model size to achieve a tradeoff between complexity and performance. In this subsection, we showcase the impact of changing the number of iterations L and the feature dimension d . Our evaluations are conducted using Rayleigh fading channel with $(N_r, N_t) = (64, 32)$ and 64-QAM modulation.

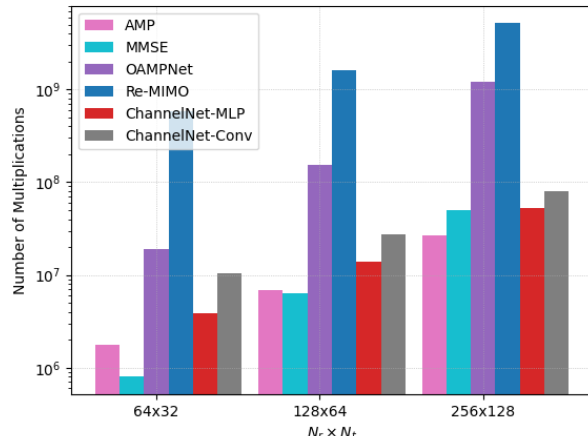
The performance of different configurations of L and d is depicted in Fig. 6 (a). When comparing with the model having $d = 10$ and $L = 20$, which is used in all previous experiments, we observe a slight performance improvement by increasing d to 20, bringing it closer to the ML bound. However, a notable drop in performance occurs when both L is reduced to 10. Significantly, the performance appears to be more sensitive to changes in L than in d , as indicated by the substantial performance difference between $d = 20$ and $L = 10$ compared to $d = 10$ and $L = 20$.

E. Computational Complexity Comparison

In this subsection, we conduct a comparison of the computational complexity between ChannelNet and existing detectors. As discussed in Section III, the computational complexity of ChannelNet is $\mathcal{O}(N_r N_t)$. Going beyond the \mathcal{O} analysis,



(a)



(b)

Fig. 6: (a) Tradeoff between model size and performance. (b) Computation complexity comparison under different antenna configurations.

we compare the number of multiplications required by these detectors in our experiments. Fig. 6 (b) illustrates the number of multiplications needed with varying numbers of transmit and receive antennas.

From the figure, it is observed that the number of multiplications for ChannelNet-MLP is approximately 2-3 times larger than for AMP, both having $\mathcal{O}(N_r N_t)$ complexity. MMSE requires the fewest multiplications when the number of antennas is small, but its growth becomes more rapid with an increasing number of antennas, following $\mathcal{O}(N_r^3)$ complexity.

OAMP and Re-MIMO are more computationally intensive compared to ChannelNet, requiring approximately 10 times and 100 times more multiplications, respectively, than ChannelNet-MLP. Additionally, the number of multiplications required by ChannelNet-Conv is around 2 times more compared to ChannelNet-MLP with 64×32 antennas, but the gap reduces as the number of antennas increases.

VI. CONCLUSION AND FUTURE DIRECTIONS

In this paper, we present ChannelNet, a purely data-driven deep learning based massive MIMO detector. In contrast with model-driven approaches, ChannelNet breaks free from conventional iterative frameworks and assumptions about channel and noise distribution. ChannelNet demonstrates its effectiveness from both theoretical and empirical standpoints. Theoretically, it exhibits the capability to approximate any permutation-equivariant function in probability. Empirically, it consistently matches or surpasses the performance of existing state-of-the-art detectors and shows better robustness in various scenarios.

ChannelNet demonstrates the effectiveness of purely data-driven detectors in massive MIMO scenarios. Future research could delve deeper into exploring advanced efficient deep learning architectures beyond MLP and convolutional networks. Investigating the application of ChannelNet to address

practical challenges, such as hardware constraints, in a data-driven manner would also be valuable. Furthermore, extending the application of ChannelNet to similar communication systems, such as the millimeter Wave communications, offers another intriguing venue for further research.

APPENDIX A PROOF OF THEOREM 1

In the subsequent proof, for simplicity, we assume that the individual antenna feature processing function may take all continuous functions on given domains, following the settings in [28]. This assurance is provided by the universal approximation properties of MLP [23], [29]. The proof assumes the output dimension for each antenna is 1 dimension, and it can be readily extended to high-dimensional output scenarios by separately considering each dimension.

The set of all continuous permutation-equivariant functions from space X to \mathbb{R}^K is denoted as $\mathcal{C}_E(X, \mathbb{R}^K)$, the set of all continuous functions as $\mathcal{C}(X, \mathbb{R}^K)$, and the set of functions that can be represented via ChannelNet as $\mathcal{F}_C(X, \mathbb{R}^K)$ or simply \mathcal{F}_C when no confusion arises.

The separation power of a set of function \mathcal{F} is defined by the equivalence relation, where the points that cannot be separated by \mathcal{F} are considered to be equivalent. Formally, we have the following definition.

Definition 3 Let \mathcal{F} be a set of functions f defined on a set X . The equivalence relation $\rho(\mathcal{F})$ defined by, for any $x, x' \in X$,

$$(x, x') \in \rho(\mathcal{F}) \Leftrightarrow \forall f \in \mathcal{F}, f(x) = f(x'). \quad (20)$$

For a specific function f , we write $\rho(f)$ for $\rho(\{f\})$.

The Stone-Weierstrass theorem presented below serves as the primary mathematical tool in the proof. Notably, the Stone-Weierstrass theorem is tailored for equivariant functions [28], and diverse versions of this theorem can be found in [30].

Theorem 2 (Stone-Weierstrass Theorem [28]) *Let X be a compact space, $Z = \mathbb{R}^p$ for some p , G be a finite group acting (continuously) on X and Z and $\mathcal{F} \subseteq \mathcal{C}_E(X, Z)$ a (non-empty) set of equivariant functions. Denote by $\pi : Z \rightarrow Z/G$ the canonical projection on the quotient space Z/G . Consider the following assumptions,*

- 1) \mathcal{F} is a sub-algebra of $\mathcal{C}(X, Z)$, and the constant function $\mathbf{1}$ is in \mathcal{F} .
- 2) The set of functions $\mathcal{F}_{scal} \subseteq \mathcal{C}(X, \mathbb{R})$ defined by $\mathcal{F}_{scal} = \{f \in \mathcal{C}(X, \mathbb{R}) : f\mathbf{1} \in \mathcal{F}\}$, satisfy $\rho(\mathcal{F}_{scal}) \subseteq \rho(\pi \circ \mathcal{F})$.

Then the closure of \mathcal{F} is

$$\bar{\mathcal{F}} = \{f \in \mathcal{C}_E(X, Z) : \rho(\mathcal{F}) \subseteq \rho(f), \forall x \in X, f(x) \in \mathcal{F}(x)\}$$

where $\mathcal{F}(x) = \{f(x), f \in \mathcal{F}\}$. Moreover, if $I(x) = \{(i, j) \in [p]^2 : \forall \mathbf{z} \in \mathcal{F}(x), \mathbf{z}_i = \mathbf{z}_j\}$, then we have $\mathcal{F}(x) = \{\mathbf{z} \in \mathbb{R}^p : \forall (i, j) \in I(x), \mathbf{z}_i = \mathbf{z}_j\}$.

As demonstrated in the example in Section IV, there exists $(\mathbf{H}, \mathbf{y}), (\hat{\mathbf{H}}, \hat{\mathbf{y}}) \in \mathbb{R}^{N \times (K+1)}$ on which ChannelNet cannot distinguish. To apply the Stone-Weierstrass theorem, we consider a subset $X_s \in \mathbb{R}^{(N \times K)} \times \mathbb{R}^N$, where

$$X_s = \{(\mathbf{H}, \mathbf{y}) \mid \mathbf{H}_{ij} \neq 0, \sum_{i=1}^N \mathbf{H}_{ij} \neq 0, \forall i, j, \mathbf{y}_k \neq \mathbf{y}_l, \forall k \neq l\}.$$

The subsequent lemmas are employed to verify that the conditions in the Stone-Weierstrass theorem are met.

Lemma 1 \mathcal{F}_C is a subalgebra of $\mathcal{C}(X_s, \mathbb{R}^K)$.

Proof of Lemma 1: It suffices to show that \mathcal{F}_C is closed under addition and multiplication. Consider any $f, \hat{f} \in \mathcal{F}_C$, where f is composed of L iterations of antenna processors, denoted by $\{\phi^{(1)}(\cdot), \dots, \psi^{(L)}(\cdot)\}$ and \hat{f} is composed of \hat{L} iterations of antenna processors, denoted by $\{\hat{\phi}^{(1)}(\cdot), \dots, \hat{\psi}^{(\hat{L})}(\cdot)\}$. First we consider the case that f and \hat{f} have the same number of iterations, i.e., $L = \hat{L}$. We can construct the $f + \hat{f}$ and $f * \hat{f}$ as follows:

- For the input receive antenna processor:

$$\phi_+^{(1)}(y) = \phi_*^{(1)}(y) = (\phi(y), \hat{\phi}(y)). \quad (21)$$

- For $\psi_+^{(i)}(\cdot)$ with $1 \leq i < L$, and $\phi_+^{(j)}(\cdot)$ with $1 < j \leq L$:

$$\psi_+^{(i)}(\mathbf{f}^{rx}, \hat{\mathbf{f}}^{rx}) = \psi_*^{(i)}(\mathbf{f}^{rx}, \hat{\mathbf{f}}^{rx}) = (\psi^{(i)}(\mathbf{f}^{rx}), \hat{\psi}^{(i)}(\hat{\mathbf{f}}^{rx})).$$

$$\phi_+^{(j)}(\mathbf{f}^{tx}, \hat{\mathbf{f}}^{tx}) = \phi_*^{(j)}(\mathbf{f}^{tx}, \hat{\mathbf{f}}^{tx}) = (\phi^{(j)}(\mathbf{f}^{tx}), \hat{\phi}^{(j)}(\hat{\mathbf{f}}^{tx})).$$

- For the output layer:

$$\psi_+^{(L)}(\mathbf{f}^{rx}, \hat{\mathbf{f}}^{rx}) = \psi^{(L)}(\mathbf{f}^{rx}) + \hat{\psi}^{(L)}(\hat{\mathbf{f}}^{rx}) \quad (22)$$

$$\psi_*^{(L)}(\mathbf{f}^{rx}, \hat{\mathbf{f}}^{rx}) = \psi^{(L)}(\mathbf{f}^{rx}) * \hat{\psi}^{(L)}(\hat{\mathbf{f}}^{rx}) \quad (23)$$

In this way, it holds

$$(f + \hat{f})(\mathbf{H}, \mathbf{y}) = f(\mathbf{H}, \mathbf{y}) + \hat{f}(\mathbf{H}, \mathbf{y}) \quad (24)$$

$$(f * \hat{f})(\mathbf{H}, \mathbf{y}) = f(\mathbf{H}, \mathbf{y}) * \hat{f}(\mathbf{H}, \mathbf{y}). \quad (25)$$

This construction satisfies $f + \hat{f} \in \mathcal{F}_C$ and $f * \hat{f} \in \mathcal{F}_C$.

Now, consider the case where $L \neq \hat{L}$, assuming $L < \hat{L}$ without loss of generality. We aim to show the existence of an equivalent function $\tilde{f} \in \mathcal{F}_C$ with \hat{L} layers, such that $\tilde{f} = f$.

To construct \tilde{f} , we leverage skip connections:

- For $1 < i \leq L$, set $\tilde{\phi}^{(i)}(\cdot) = \phi^{(i)}(\cdot)$ and $\tilde{\psi}^{(i)}(\cdot) = \psi^{(i)}(\cdot)$.
- For $L < i \leq \hat{L}$, set $\tilde{\phi}^{(i)}(\cdot) = \mathbf{0}$ and $\tilde{\psi}^{(i)}(\cdot) = \psi^{(L)}(\cdot)$.

This construction does not change the transmit and receive antenna feature processors for $1 < i \leq L$, resulting in identical features. For iterations $L + 1$ to \hat{L} , the transmit processor's input remains the same as in the L -th iteration, and the output mimics the L -th iteration's transmit features.

By substituting \hat{f} with \tilde{f} , we reduce the problem to the first case we considered, where closure under addition and multiplication was demonstrated. This concludes the proof. ■

Lemma 2 $\rho(\mathcal{F}_C) = \{(x, \sigma_{rx}(x)), x \in X_s, \sigma_{rx} \in \mathcal{S}_N\}$.

Proof of Lemma 2: To prove this lemma, we establish the equivalence between the following two conditions for any $(\mathbf{H}, \mathbf{y}), (\hat{\mathbf{H}}, \hat{\mathbf{y}}) \in X_s$:

- 1) For any function $f \in \mathcal{F}_C$, we have $f(\mathbf{H}, \mathbf{y}) = f(\hat{\mathbf{H}}, \hat{\mathbf{y}})$.
- 2) There exists $\sigma_{rx} \in \mathcal{S}_N$, such that $(\mathbf{H}, \mathbf{y}) = \sigma_{rx}(\hat{\mathbf{H}}, \hat{\mathbf{y}})$.

2) \Rightarrow 1): If σ_{rx} exists such that $(\mathbf{H}, \mathbf{y}) = \sigma_{rx}(\hat{\mathbf{H}}, \hat{\mathbf{y}})$, then for any $f \in \mathcal{F}_C$, we have $\mathbf{F}_{rx} = \sigma_{rx}(\hat{\mathbf{F}}_{rx})$ and $\mathbf{F}_{tx} = \hat{\mathbf{F}}_{tx}$ for each iteration. Therefore we can conclude that $\forall f \in \mathcal{F}_C$, $f(\mathbf{H}, \mathbf{y}) = f(\hat{\mathbf{H}}, \hat{\mathbf{y}})$.

1) \Rightarrow 2): If no $\sigma_{rx} \in \mathcal{S}_K$ exists, such that $(\mathbf{H}, \mathbf{y}) = \sigma_{rx}(\hat{\mathbf{H}}, \hat{\mathbf{y}})$, we consider two cases:

- 1) There exists no $\sigma_{rx} \in \mathcal{S}_K$ such that $\mathbf{y} = \sigma_{rx}(\hat{\mathbf{y}})$. Since both \mathbf{y} and $\hat{\mathbf{y}}$ have distinct values, an index i exists such that $\mathbf{y}_i \neq \hat{\mathbf{y}}_j, \forall j$. Consider $f \in \mathcal{F}_C$ with 1 iteration and the following $\phi(\cdot)$ and $\psi(\cdot)$:

- $\phi(\mathbf{y}_i) = 1, \phi(\mathbf{y}_j) = 0, \forall j \neq i$, and $\phi(\hat{\mathbf{y}}_k) = 0, \forall k$.
- $\psi(0) = 0$ and $\psi(\mathbf{H}_{ij}) = 1, \forall j$.

We have $f(\mathbf{H}, \mathbf{y}) = \mathbf{1}$ while $f(\hat{\mathbf{H}}, \hat{\mathbf{y}}) = \mathbf{0}$, showing that the two inputs can be separated by f .

- 2) There exists σ_{rx} , such that $\mathbf{y} = \sigma_{rx}(\hat{\mathbf{y}})$, but $\mathbf{H} \neq \sigma_{rx}(\hat{\mathbf{H}})$. Then, let $\mathbf{G} = \sigma_{rx}(\hat{\mathbf{H}})$ and we can find indexes i such that $\mathbf{H}_{:i} \neq \mathbf{G}_{:i}$. Consider a $f \in \mathcal{F}_C$ with 1 iteration and the following $\phi(\cdot)$ and $\psi(\cdot)$:

- $\phi(\mathbf{y}_i) = 1$ and $\phi(\mathbf{y}_j) = 0, \forall j \neq i$.
- $\psi(z) = z$.

We have $f(\mathbf{H}, \mathbf{y}) = \mathbf{H}_{:i}$ while $f(\hat{\mathbf{H}}, \hat{\mathbf{y}}) = \mathbf{G}_{:i}$, showing that f separates the two inputs.

The above two cases establish that when there is no $\sigma_{rx} \in \mathcal{S}_K$ such that $(\mathbf{H}, \mathbf{y}) = \sigma_{rx}(\hat{\mathbf{H}}, \hat{\mathbf{y}})$, there exists $f \in \mathcal{F}_C$ with $f(\mathbf{H}, \mathbf{y}) \neq f(\hat{\mathbf{H}}, \hat{\mathbf{y}})$. This concludes the proof of Lemma 2. ■

Lemma 3 *There exists $\mathcal{F}_{scal} = \{f \in \mathcal{C}(X_s, \mathbb{R}) : f\mathbf{1} \in \mathcal{F}_C\}$, which satisfies $\rho(\mathcal{F}_{scal}) \subseteq \rho(\pi \circ \mathcal{F}_C)$, where π is the quotient map of σ_{tx} .*

Proof of Lemma 3: We define $\mathcal{F}_{scal} = \{f_{scal} \mid f_{scal}(x) = \sum_{i=1}^K f(x)_i, f \in \mathcal{F}_C\}$.

Now, we aim to show that for any $f_{scal} \in \mathcal{F}_{scal}$, $f_{scal}\mathbf{1}$ can be represented by a function $\hat{f} \in \mathcal{F}_C$. We construct \hat{f} using $L + 1$ iterations, where L is the number of iterations for f

corresponding to f_{scal} . Same antenna processors are adopted for the first L iterations in \hat{f} , except the $\hat{\psi}^{(L)}$ is defined as $\hat{\psi}^{(L)}(\cdot) = p \circ \psi^{(L)}(\cdot)$, where $p(z) = [1, z, z^2, \dots, z^{2K}]$ mapping input z into a vector of length $2K + 1$.

Consequently, for a given (\mathbf{H}, \mathbf{y}) , the input of the i -th receive antenna processor for the $L + 1$ iteration is:

$$\mathbf{f}_i^{rx} = \left[\sum_{j=1}^K \mathbf{H}_{ij}, \sum_{j=1}^K \mathbf{H}_{ij} \mathbf{z}_j, \dots, \sum_{j=1}^K \mathbf{H}_{ij} \mathbf{z}_j^{2K} \right],$$

where $\mathbf{z} = f(\mathbf{H}, \mathbf{y})$.

Next we show that based on \mathbf{f}_i^{rx} , we can determine the $2K$ unknowns, namely $\mathbf{H}_{:i}$ and \mathbf{z} , up to permutation.

If there are another set of real-valued solution besides $(\mathbf{z}, \mathbf{H}_{:i})$, denoted by $(\hat{\mathbf{z}}, \hat{\mathbf{h}})$, then we have

$$\sum_{j=1}^K \mathbf{H}_{ij} \mathbf{z}_j^s - \sum_{j=1}^K \hat{\mathbf{h}}_j \hat{\mathbf{z}}_j^s = 0, s \in \{0, 1, \dots, 2K\} \quad (26)$$

Consider the set of vectors $V = \{[1, z, z^2, \dots, z^{2K}] \mid z \in \mathbf{z} \text{ or } x \in \hat{\mathbf{z}}\}$. Since $(\mathbf{z}, \mathbf{H}_{:i})$ and $(\hat{\mathbf{z}}, \hat{\mathbf{h}})$ are not equal up to permutation, according to (26), there exists subset of vectors in V that are linearly dependent, which in contradict with that fact that if $z_1 \neq z_2 \dots \neq z_{2K}$, then vectors $\{[1, z_i, z_i^2, \dots, z_i^{2K}]\}$ are linearly independent. As a result, $(\mathbf{z}, \mathbf{H}_{:i})$ is the only real-value solution up to permutation. Hence, the map from \mathbf{f}_i^{rx} to $\sum_{j=1}^K \mathbf{z}_j$ is unique and continuous, therefore we can choose $\phi^{(L+1)}(\cdot)$ to map \mathbf{f}_i^{rx} to a two dimensional vector $(1, \sum_{j=1}^K \mathbf{z}_j)$, and \mathbf{f}_k^{tx} after the channel layer becomes $(\sum_{l=1}^N \mathbf{H}_{lk}, \sum_{l=1}^N \mathbf{H}_{lk} \sum_{j=1}^K \mathbf{z}_j)$, $\psi^{(L+1)}(\cdot)$ calculate the division of second value over the first value can obtain the desired $\sum_{i=1}^K \mathbf{z}_i$. Therefore, $f_{scal} \mathbf{1} \in \mathcal{F}_C$.

To prove $\rho(\mathcal{F}_{scal}) \subseteq \rho(\pi \circ \mathcal{F}_C)$, we establish the following conditions are equivalent for any $(\mathbf{H}, \mathbf{y}), (\hat{\mathbf{H}}, \hat{\mathbf{y}}) \in X_s$:

- 1) $f(\mathbf{H}, \mathbf{y}) = f(\hat{\mathbf{H}}, \hat{\mathbf{y}}), \forall f \in \mathcal{F}_{scal}$.
- 2) There exists $\sigma_{rx} \in \mathcal{S}_N$ and $\sigma_{tx} \in \mathcal{S}_K$ such that $(\mathbf{H}, \mathbf{y}) = (\sigma_{rx} * \sigma_{tx})(\hat{\mathbf{H}}, \hat{\mathbf{y}})$.
- 2) \Rightarrow 1): If such σ_{rx} and σ_{tx} exist, we have

$$\begin{aligned} f_{scal}(\mathbf{H}, \mathbf{y}) &= \sum_{i=1}^K f((\sigma_{rx} * \sigma_{tx})(\hat{\mathbf{H}}, \hat{\mathbf{y}}))_i \stackrel{(1)}{=} \sum_{i=1}^K \sigma_{tx}(f(\hat{\mathbf{H}}, \hat{\mathbf{y}}))_i \\ &\stackrel{(2)}{=} \sum_{i=1}^K f(\hat{\mathbf{H}}, \hat{\mathbf{y}})_i = f_{scal}(\hat{\mathbf{H}}, \hat{\mathbf{y}}), \end{aligned}$$

where (1) is due to $\rho(\mathcal{F}_C) = \{(x, \sigma_{rx}(x)), x \in X_s, \sigma_{rx} \in \mathcal{S}_K\}$ and (2) is due to the sum function being independent of the order of inputs.

1) \Rightarrow 2): If there doesn't exist σ_{rx} and σ_{tx} such that $(\mathbf{H}, \mathbf{y}) = (\sigma_{rx} * \sigma_{tx})(\hat{\mathbf{H}}, \hat{\mathbf{y}})$, two cases are considered:

- 1) If no σ_{rx} exists such that $\mathbf{y} = \sigma_{rx}(\hat{\mathbf{y}})$, consider the same example in the first condition in the proof of Lemma 2. We have $f(\mathbf{H}, \mathbf{y}) = \mathbf{0}$ while $f(\hat{\mathbf{H}}, \hat{\mathbf{y}}) = \mathbf{1}$. Thus for f_{scal} of f , we have $f_{scal}(\mathbf{H}, \mathbf{y}) \neq f_{scal}(\hat{\mathbf{H}}, \hat{\mathbf{y}})$.
- 2) If σ_{rx} exists such that $\mathbf{y} = \sigma_{rx}(\hat{\mathbf{y}})$, but there is no σ_{tx} such that $\mathbf{H} = \sigma_{tx}(\mathbf{G})$, where $\mathbf{G} = \sigma_{rx}(\mathbf{H})$, then there exists index sets $I, J \subseteq [K]$ for \mathbf{H} and \mathbf{G} , respectively,

with a one-to-one match between their columns within the corresponding index set. However, for any column in \mathbf{H} that is outside of I , there is no match to columns in \mathbf{G} outside of J , i.e., $\mathbf{H}_{:i} \neq \mathbf{G}_{:j}, \forall i \notin I, j \notin J$. Since there is no σ_{tx} such that $\mathbf{H} = \sigma_{tx}(\mathbf{G})$, we can always find a index $i \notin I$. Let k denote the number of rows of \mathbf{H} inside of I that are equal to $\mathbf{H}_{:i}$. Consider $f \in \mathcal{F}_C$ with a single iteration and the following $\phi(\cdot)$ and $\psi(\cdot)$:

- $\phi(\mathbf{y}_i) = \mathbf{e}_i$, where $\mathbf{e}_i = [0, 0, \dots, 1, \dots, 0]$ with only the i -th item being 1.
- $\psi(\mathbf{H}_{:i}) = 1, \psi(\mathbf{H}_{:j}) = 0, \forall \mathbf{H}_{:j} \neq \mathbf{H}_{:i}$, and $\psi(\mathbf{G}_{:j}) = 0, \forall \mathbf{G}_{:j} \neq \mathbf{H}_{:i}$.

We have $\sum_{j=1}^K f(\mathbf{H}, \mathbf{y})_j = k+1$ and $\sum_{j=1}^K f(\hat{\mathbf{H}}, \hat{\mathbf{y}})_j = k$. For f_{scal} of f , we have $f_{scal} \neq f_{scal}(\hat{\mathbf{H}}, \hat{\mathbf{y}})$.

The above two cases establish that if there are no σ_{rx} and σ_{tx} such that $(\mathbf{H}, \mathbf{y}) = (\sigma_{rx} * \sigma_{tx})(\hat{\mathbf{H}}, \hat{\mathbf{y}})$, then there exists $f_{scal} \in \mathcal{F}_{scal}$, such that $f_{scal}(\mathbf{H}, \mathbf{y}) \neq f_{scal}(\hat{\mathbf{H}}, \hat{\mathbf{y}})$, which concludes the proof of Lemma 3. ■

With the above three lemmas, we have the following lemma characterizing the representation power of \mathcal{F}_C .

Lemma 4 For any compact $W \subseteq X_c, \bar{\mathcal{F}}_C = \mathcal{C}_E(W, \mathbb{R}^K)$.

Proof of Lemma 4: Let $G = \mathcal{S}_K$. Applying the Stone-Weierstrass Theorem, we have

- Condition 1 follows from Lemma 1.
- Condition 2 follows from Lemma 3.

Therefore, according the theorem, the closure of \mathcal{F}_C is

$$\begin{aligned} \bar{\mathcal{F}}_C &= \{h \in \mathcal{C}_E(W, \mathbb{R}^K) : \rho(\mathcal{F}_C) \subseteq \rho(h), \\ &\quad \forall (\mathbf{H}, \mathbf{y}) \in W, h(\mathbf{H}, \mathbf{y}) \in \mathcal{F}_C(\mathbf{H}, \mathbf{y})\}, \end{aligned}$$

where $\mathcal{F}_C(\mathbf{H}, \mathbf{y}) = \{f(\mathbf{H}, \mathbf{y}), f \in \mathcal{F}_C\} = \{\mathbf{z} \in \mathbb{R}^K : \forall (i, j) \in I(\mathbf{H}, \mathbf{y}), \mathbf{z}_i = \mathbf{z}_j\}$ and $I(\mathbf{H}, \mathbf{y}) = \{(i, j) \in [K]^2 : \forall f \in \mathcal{F}_C, f(\mathbf{H}, \mathbf{y})_i = f(\mathbf{H}, \mathbf{y})_j\}$.

Next, we are going remove the two conditions.

From Lemma 2, we have $\rho(\mathcal{F}_C) = \{(x, \sigma_{rx}(x)), x = (\mathbf{H}, \mathbf{y}) \in W, \sigma_{rx} \in \mathcal{S}_N\}$. According to Definition 2, for every $h \in \mathcal{C}_E(W, \mathbb{R}^K)$, we have $\rho(\mathcal{F}_C) \subseteq \rho(h)$.

Consider functions $\mathcal{F}_H = \{f_m \in \mathcal{F}_C, m \in [N]\}$, each with a single iteration defined by $\phi_m(\cdot)$ and $\psi_m(\cdot)$:

- $\phi_m(\mathbf{y}_m) = 1, \phi_m(\mathbf{y}_n) = 0, \forall n \neq m$
- $\psi_m(z) = z$.

The output of $f_m(\mathbf{H}, \mathbf{y}) = \mathbf{H}_{:m}$. Denote $I_H(\mathbf{H}, \mathbf{y}) = \{(i, j) \in [K]^2, f(\mathbf{H}, \mathbf{y})_i = f(\mathbf{H}, \mathbf{y})_j, \forall f \in \mathcal{F}_H\}$, then $I(\mathbf{H}, \mathbf{y}) \subseteq I_H(\mathbf{H}, \mathbf{y})$. If $(i, j) \in I_H(\mathbf{H}, \mathbf{y})$, we have $\mathbf{H}_{:i} = \mathbf{H}_{:j}$, implying the existence of a permutation $\sigma_{tx} \in \mathcal{S}_K$ that switches i and j , such that $\mathbf{H} = \sigma_{tx}(\mathbf{H})$. Therefore, for any $h \in \mathcal{C}_E(W, \mathbb{R}^K)$, we have $h(\mathbf{H}, \mathbf{y})_i = \sigma_{tx}(h(\mathbf{H}, \mathbf{y}))_j = h(\sigma_{tx}(\mathbf{H}), \mathbf{y})_j = h(\mathbf{H}, \mathbf{y})_j$. Since $\mathcal{F}_H \subseteq \mathcal{F}_C$, $I(\mathbf{H}, \mathbf{y}) \subseteq I_H(\mathbf{H}, \mathbf{y})$, we conclude that $h(\mathbf{H}, \mathbf{y}) \in \mathcal{F}_C(\mathbf{H}, \mathbf{y})$.

Hence, $\bar{\mathcal{F}}_C = \mathcal{C}_E(W, \mathbb{R}^K)$. ■

Proof of Theorem 1: For any Boral probability measure P on $\mathbb{R}^{N \times (K+1)}$, the complement $\mathbb{R}^{N \times (K+1)} \setminus X_s$ consists only of sub-spaces that have measure zero, namely, implying that the measure of X_s is 1. Thus, for any given δ , we can find a compact subset $W \in X_s$ such that $P(W) > 1 - \delta$. By applying Lemma 4, for any given $g \in \mathcal{C}_E(W, \mathbb{R}^K)$, and any $\epsilon > 0$, there

exists $f \in \mathcal{F}_C(W, \mathbb{R}^K)$, such that $\|f(\mathbf{H}, \mathbf{y}) - g(\mathbf{H}, \mathbf{y})\| < \epsilon, \forall (\mathbf{H}, \mathbf{y}) \in W$, which concludes the proof. ■

APPENDIX B PROOF OF COROLLARY

Lemma 5 f_{ML} is measurable and permutation-equivariant.

Proof of Lemma 5: Consider the distance function for a given pair (\mathbf{H}, \mathbf{y}) , defined as $d_{(\mathbf{H}, \mathbf{y})}(\mathbf{x}) = \|\mathbf{H}\mathbf{x} - \mathbf{y}\|_2^2$. The ML detector f_{ML} is expressed as $f_{ML}(\mathbf{H}, \mathbf{y}) = \arg \min_{\mathbf{x} \in \mathcal{X}^K} (d_{(\mathbf{H}, \mathbf{y})}(\mathbf{x}))$. For any $\sigma_{rx} \in \mathcal{S}_N$ with a corresponding permutation matrix $\mathbf{P}_{rx} \in \{0, 1\}^{N \times N}$, we have

$$\begin{aligned} d_{(\sigma_{rx}(\mathbf{H}, \mathbf{y}))}(\mathbf{x}) &= \|\mathbf{P}_{rx}\mathbf{H}\mathbf{x} - \mathbf{P}_{rx}\mathbf{y}\|_2^2 = \|\mathbf{P}_{rx}(\mathbf{H}\mathbf{x} - \mathbf{y})\|_2^2 \\ &= \|\mathbf{P}_{rx}\|_2^2 \|\mathbf{H}\mathbf{x} - \mathbf{y}\|_2^2 = d_{(\mathbf{H}, \mathbf{y})}(\mathbf{x}), \end{aligned}$$

which shows the equality of $d_{(\mathbf{H}, \mathbf{y})}(\cdot)$ and $d_{(\sigma_{rx}(\mathbf{H}, \mathbf{y}))}(\cdot)$. Therefore, we conclude that $f_{ML}(\mathbf{H}, \mathbf{y}) = f_{ML}(\sigma_{rx}(\mathbf{H}, \mathbf{y}))$.

Now, consider any $\sigma_{tx} \in \mathcal{S}_K$ with a corresponding permutation matrix $\mathbf{P}_{tx} \in \{0, 1\}^{K \times K}$. We have

$$\begin{aligned} d_{(\sigma_{tx}(\mathbf{H}, \mathbf{y}))}(\mathbf{x}) &= \|\sigma_{tx}(\mathbf{H})\mathbf{x} - \mathbf{y}\|_2^2 \\ &= \|\mathbf{H}\mathbf{P}_{tx}\mathbf{x} - \mathbf{y}\|_2^2 = d_{(\mathbf{H}, \mathbf{y})}(\sigma_{tx}(\mathbf{x})). \end{aligned}$$

This establishes $f_{ML}(\sigma_{tx}(\mathbf{H}), \mathbf{y}) = \sigma_{tx}(f_{ML}(\mathbf{H}, \mathbf{y}))$. Hence, we can conclude f_{ML} is a permutation-equivariant function.

To demonstrate f_{ML} being measurable, it is sufficient to establish that the preimage of each point in \mathcal{X}^K is measurable. For any $\mathbf{x} \in \mathcal{X}^K$, consider the function $g_{\mathbf{x}} : \mathbb{R}^{N \times (K+1)} \rightarrow \mathbb{R}$:

$$g_{\mathbf{x}}(\mathbf{H}, \mathbf{y}) = \|\mathbf{H}\mathbf{x} - \mathbf{y}\|_2^2 - \min_{\mathbf{z} \in \mathcal{X}^K} \|\mathbf{H}\mathbf{z} - \mathbf{y}\|_2^2. \quad (27)$$

$g_{\mathbf{x}}$ is continuous due to the continuity of the norm, and therefore measurable. Since $f_{ML}^{-1}(\mathbf{x}) = g_{\mathbf{x}}^{-1}(0)$ and $g_{\mathbf{x}}^{-1}(0)$ is measurable, we conclude that $f_{ML}^{-1}(\mathbf{x})$ is measurable, thereby establishing f_{ML} as a measurable function. ■

With the following Lusin's theorem, f_{ML} being measurable is sufficient for the proof of the Corollary.

Theorem 3 (Lusin's theorem [29]) *Let $f : X \rightarrow \mathbb{R}$ be a measurable function defined on a Lebesgue measurable set $X \subseteq \mathbb{R}^p$ for which the Lebesgue measure $l(X)$ is finite. Then for each $\delta > 0$ there exists a compact subset $W \subseteq X$ such that $l(X \setminus W) < \delta$ and f is continuous on W .*

Proof of Corollary: From Lemma 5, f_{ML} is measurable and permutation-equivariant. Consider any Borel probability measure P on $\mathbb{R}^{N \times (K+1)}$. According to Lusin's theorem, for any δ , there exists a compact subset $W \subseteq X_s$ such that $P(W) > 1 - \delta$ and f_{ML} is continuous on W . According to Lemma 4, for any given ϵ , there exists $f \in \mathcal{F}_C$, such that $\|f(x) - f_{ML}(x)\| < \epsilon, \forall x \in W$, which concludes the proof. ■

REFERENCES

- [1] A. J. Paulraj, D. A. Gore, R. U. Nabar, and H. Bolcskei, "An overview of MIMO communications—a key to gigabit wireless," *Proc. IEEE*, vol. 92, no. 2, pp. 198–218, Feb. 2004.
- [2] L. Lu, G. Y. Li, A. L. Swindlehurst, A. Ashikhmin, and R. Zhang, "An overview of massive MIMO: Benefits and challenges," *IEEE J. Sel. Topics Signal Process.*, vol. 8, no. 5, pp. 742–758, Oct. 2014.
- [3] S. Yang and L. Hanzo, "Fifty years of mimo detection: The road to large-scale mimos," *IEEE Communications Surveys & Tutorials*, vol. 17, no. 4, pp. 1941–1988, 2015.
- [4] E. G. Larsson, "MIMO detection methods: How they work," *IEEE Signal Process. Mag.*, vol. 26, no. 3, pp. 91–95, May 2009.
- [5] J. Ma and L. Ping, "Orthogonal amp," *IEEE Access*, vol. 5, pp. 2020–2033, 2017.
- [6] H. He, C.-K. Wen, S. Jin, and G. Y. Li, "Model-driven deep learning for MIMO detection," *IEEE Trans. Signal Process.*, vol. 68, pp. 1702–1715, 2020.
- [7] M. Khani, M. Alizadeh, J. Hoydis, and P. Fleming, "Adaptive neural signal detection for massive MIMO," *IEEE Trans. Wireless Commun.*, vol. 19, no. 8, pp. 5635–5648, Aug. 2020.
- [8] M. Goutay, F. A. Aoudia, and J. Hoydis, "Deep hypernetwork-based mimo detection," in *Proc. IEEE 21st Int. Workshop Signal Process. Adv. Wireless Commun. (SPAWC)*, Jul. 2020, pp. 1–5.
- [9] V. Monga, Y. Li, and Y. C. Eldar, "Algorithm unrolling: Interpretable, efficient deep learning for signal and image processing," *IEEE Signal Process. Mag.*, vol. 38, no. 2, pp. 18–44, Mar. 2021.
- [10] N. Zilberstein, C. Dick, R. Doost-Mohammady, A. Sabharwal, and S. Segarra, "Annealed langevin dynamics for massive MIMO detection," *IEEE Trans. Wireless Commun.*, vol. 22, no. 6, pp. 3762–3776, Jun. 2023.
- [11] N. Samuel, T. Diskin, and A. Wiesel, "Deep mimo detection," in *Proc. IEEE 18th Int. Workshop Signal Process. Adv. Wireless Commun. (SPAWC)*, Jul. 2017, pp. 1–5.
- [12] K. Pratik, B. D. Rao, and M. Welling, "RE-MIMO: Recurrent and permutation equivariant neural mimo detection," *IEEE Trans. Signal Process.*, vol. 69, pp. 459–473, 2020.
- [13] Q. Hu, F. Gao, H. Zhang, G. Y. Li, and Z. Xu, "Understanding deep MIMO detection," *IEEE Trans. Wireless Commun.*, vol. 22, no. 12, pp. 9626–9639, Dec. 2023.
- [14] C. Jeon, R. Ghods, A. Maleki, and C. Studer, "Optimality of large mimo detection via approximate message passing," in *Proc. IEEE Int. Symp. Inf. Theory (ISIT)*, Jun. 2015, pp. 1227–1231.
- [15] A. M. Tulino, S. Verdú *et al.*, "Random matrix theory and wireless communications," *Foundations and Trends® in Communications and Information Theory*, vol. 1, no. 1, pp. 1–182, 2004.
- [16] A. Wiesel, Y. C. Eldar, and S. Shamai, "Semidefinite relaxation for detection of 16-qam signaling in MIMO channels," *IEEE Signal Process. Lett.*, vol. 12, no. 9, pp. 653–656, Sep. 2005.
- [17] Z. Guo and P. Nilsson, "Algorithm and implementation of the k-best sphere decoding for MIMO detection," *IEEE J. Sel. Areas Commun.*, vol. 24, no. 3, pp. 491–503, Mar. 2006.
- [18] A. Beck and M. Teboulle, "A fast iterative shrinkage-thresholding algorithm for linear inverse problems," *SIAM J. Imag. Sci.*, vol. 2, no. 1, pp. 183–202, Mar. 2009.
- [19] P. Putzky and M. Welling, "Recurrent inference machines for solving inverse problems," *arXiv preprint arXiv:1706.04008*, 2017.
- [20] M. Zaheer, S. Kottur, S. Ravanbakhsh, B. Poczos, R. R. Salakhutdinov, and A. J. Smola, "Deep sets," *Proc. Adv. Neural Inf. Process. Syst. (NeurIPS)*, pp. 3391–3401, Dec. 2017.
- [21] C. R. Qi, H. Su, K. Mo, and L. J. Guibas, "Pointnet: Deep learning on point sets for 3d classification and segmentation," in *Proc. IEEE Conf. Comput. Vis. Pattern Recognit. (CVPR)*, Jul. 2017, pp. 652–660.
- [22] K. He, X. Zhang, S. Ren, and J. Sun, "Deep residual learning for image recognition," in *Proc. IEEE Conf. Comput. Vis. Pattern Recognit. (CVPR)*, Jul. 2016, pp. 770–778.
- [23] G. Cybenko, "Approximation by superpositions of a sigmoidal function," *Math. Control Signals Syst.*, vol. 2, no. 4, pp. 303–314, Dec. 1989.
- [24] K. Hornik, M. Stinchcombe, and H. White, "Multilayer feedforward networks are universal approximators," *Neural networks*, vol. 2, no. 5, pp. 359–366, Mar. 1989.
- [25] G. Optimization *et al.*, "Gurobi optimizer reference manual," 2020.
- [26] D. P. Kingma and J. Ba, "Adam: A method for stochastic optimization," *arXiv preprint arXiv:1412.6980*, 2014.
- [27] S. L. Loyka, "Channel capacity of mimo architecture using the exponential correlation matrix," *IEEE Commun. Lett.*, vol. 5, no. 9, pp. 369–371, Sep. 2001.
- [28] W. Azizian and M. Lelarge, "Expressive power of invariant and equivariant graph neural networks," *arXiv preprint arXiv:2006.15646*, 2020.
- [29] L. Evans, *Measure theory and fine properties of functions*. Routledge, 2018.
- [30] V. Timofte, "Stone-weierstrass theorems revisited," *Journal of Approximation Theory*, vol. 136, no. 1, pp. 45–59, 2005.